

How much N-doping can Graphene Sustain?

Zhiming Shi^{1,2}, Alex Kutana² and Boris I. Yakobson^{*2,3}

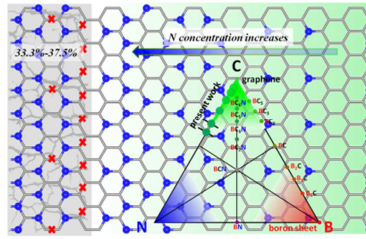
¹The State Key Laboratory of Theoretical and Computational Chemistry, Institute of Theoretical Chemistry, Jilin University, Changchun 130023, People's Republic of China

²Department of Materials Science and Nanoengineering, Rice University, Houston, Texas 77005, USA

³Department of Chemistry, Rice University, Houston, Texas 77005, USA

Abstract

Doped, substituted, or alloyed graphene is an attractive candidate for use as a tunable element of future nanomechanical and optoelectronic devices. Here we use the density-functional theory, density functional tight binding, cluster expansion, and molecular dynamics to investigate the thermal stability and electronic properties of a binary 2D graphene-like alloy of carbon and nitrogen ($C_{1-x}N_x$). The stability range naturally begins from graphene, and must certainly end before $x = 1$, where pure nitrogen rather forms molecular gas. This poses a compelling question of what highest $x < 1$ still permits stable 2D hexagonal lattice. Such upper limit on the nitrogen concentration that is achievable in a stable alloy can be found based on the phonon and molecular dynamics calculations. The stability switchover is predicted to be between $x=1/3$ (33.3%) and $x=3/8$ (37.5%), and no stable hexagonal lattice two-dimensional CN alloys can exist at the N concentration of $x=3/8$ (37.5%) and higher.



TOC

Keywords: two-dimensional CN alloy, stability, maximum N concentration, phonon spectrum and molecular dynamics

Doping and alloying are powerful techniques for tailoring mechanical, electronic, optical, and other properties of materials. Recently, there has been a great interest in doping and alloying of the new one-layer-thick two-dimensional (2D) materials, by both experimentalists and theorists.¹⁻⁴ In graphene, substitutional doping and alloying with various elements such as boron, nitrogen, sulfur, and silicon, are possible.⁴⁻¹⁰ Two-dimensional alloys of carbon, boron and nitrogen are especially interesting, due to potential for extending applications of pure graphene and two-dimensional boron nitride (BN).¹¹⁻²² It is convenient to represent the mixing diagram of these ternary alloys by a Gibbs triangle, as shown in Fig. 1. Each corner of the triangle represents a pure compound, and contents of pure substances in a mixed compound are proportional to distances from the point within the triangle to bases opposing the corners for the corresponding pure substances. Substitutional doping of graphene would correspond to the sides starting from the C corner of the triangle. Various electronic properties of homogeneous BCN alloys have been explored theoretically,^{14,19,22} although experimental works have indicated that uniformity may be difficult to achieve in BCN.^{18,20,21,23} Here, we explore the CN side of the BCN Gibbs triangle (highlighted in Fig. 1), i.e. graphitic nitrogen-substituted graphene (g-NG), which has become a focus of numerous research works because of its rich properties and many potential applications, including high-frequency semiconductor devices,⁵ metal-free catalyst for energy conversion and storage,²⁴⁻²⁶ chemical hydrogen storage,²⁷ Li-ion batteries²⁸, molecular sieves²⁹ and supercapacitors.³⁰ Experimentally, large scale³¹ nitrogen doped graphene (NG) have been synthesized by utilizing Chemical Vapor Deposition (CVD)³² and solvothermal synthesis,³³ using pyridine^{4,31,34} and s-triazine³⁵ as precursors. Several types of local configurations near an N atom, such as “graphitic”, “pyridinic” and “pyrrolic”, have been detected.^{10,32} Zhao *et al.* grew N-doped graphene films using CVD on a copper foil substrate, and confirmed that the individual nitrogen atoms are incorporated as graphitic dopants.⁸ By using atmospheric-pressure chemical vapor deposition (AP-CVD) method, STM/STS studies and ab initio simulations, Lv *et al.*¹⁰ have revealed that NG sheets contain an abundant amount of N dopants within the same graphene sub-lattice (e.g. 80% dominance among all the identified defects), and a novel and outstanding Raman enhancement of Rhodamine B molecules was demonstrated when using NG sheet as a substrate. Experiments suggest that nitrogen species have been incorporated into the graphene structure with the content of 16.4 at. % (13 wt. %) with solvothermal synthesis.³³ Recently, N doping graphene with even higher N contents of 18 wt. % have achieved by C. N. R. Rao et al. with microwave synthesis, and perform promising applications in supercapacitor.³⁶ They also demonstrated that the presence of nitrogen within the structure of nitrogen-doped reduced graphene oxide induces a remarkable increase in the thermal stability against oxidation by air.³⁷ Even higher nitrogen concentrations in $C_{1-x}N_x$ compounds, e.g. $x=4/7$ in C_3N_4 can be achieved,³⁸ if vacancies or terminating hydrogen atoms are admitted.³⁸⁻⁴² Here we limit our study to graphene with nitrogen substitutional defects (NG), without consideration of other types of defects, i.e.

perform a constrained search on a honeycomb (graphene) lattice with allowed site occupancies limited to C or N atoms only. Graphitic NG configurations have been widely observed as a domain type in many experiments,^{8,10,31,32,43} resulting in n-doped materials.^{44,45} In many applications, the limit of the N doping concentration in g-NG is important for both basic research and practical uses; however, it has not been found yet. Only isolated two-dimensional CN alloys were considered previously, such as $C_{12}N$ and C_3N ,¹¹ which are shown as smaller points on the diagram in Fig. 1, along with other two-dimensional BCN alloys considered theoretically.^{3,12-19} Here, we use the density-functional theory and cluster expansion to establish the theoretical limits of N doping in g-NG, and investigate its stability and electronic properties. We demonstrate that the nitrogen concentration in g-NG can in principle be as high as 33.3%-37.5%, and that most of these structures are metallic.

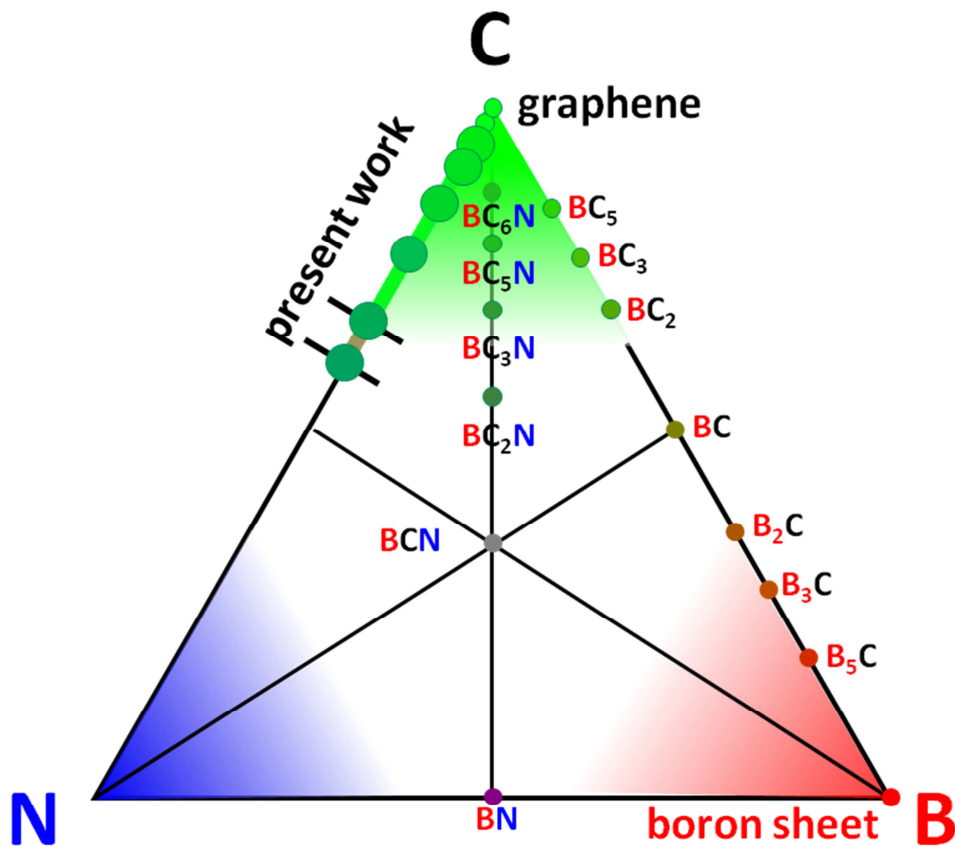


Figure 1. Gibbs triangle for the hexagonal-lattice two-dimensional BCN alloy. The highlighted edge of the triangle (CN) corresponds to nitrogen-substituted graphene, which is the focus of the current work. Large circles denote lowest-energy stable structures that were found here. The two dashes denote the

range of concentration where the stability range ends. Smaller circles show other two-dimensional BCN systems considered previously.^{3,11-19}

Mixing energies of the 2D carbon-nitrogen alloy were obtained using the cluster expansion (CE) method.⁴⁶ CE provides an efficient way to sample a M^N -dimensional configuration space of an N -site M -component alloy. Unlike mean field treatments, the CE method gives the full microscopic description of atomic configurations in a crystal. In the CE formalism, a function f of configurations $\sigma = \{\sigma_1, \sigma_2, \dots, \sigma_N\}$ of spins σ_i on N lattice sites is fitted through a multivariate expansion in site occupancy variables (spins) σ_i . In an alloy, the roles of spin variables are played by the chemical identities of different atomic species. The general cluster expansion of the function $f(\sigma)$ can be written as:⁴⁶

$$f(\sigma) = \sum_{\alpha, s} f_{\alpha s} \Phi_{\alpha s}(\sigma) \quad (1)$$

where $f_{\alpha s}$ are the expansion coefficients and $\Phi_{\alpha s}(\sigma)$ are the so-called characteristic cluster functions defined for all possible distinct subsets (clusters) $\alpha = \{p, p', \dots, p''\}$ of the points of the full lattice. The sets $s = \{n, n', \dots, n''\}$ in the sum Eq.1 include all possible non-zero indices of discrete orthonormal polynomials entering the definition of the cluster functions $\Phi_{\alpha s}(\sigma)$. Zero-index orthonormal polynomials have the value of 1, and therefore do not need to be written explicitly. As expected, the sum Eq. 1 has M^N terms.

In case of a two-component crystalline alloy, the cluster expansion of the mixing energy per lattice site can be written as:⁴⁷

$$E(\sigma) = \sum_{\alpha} m_{\alpha} J_{\alpha} \left\langle \prod_{i \in \alpha_{eq}} \sigma_i \right\rangle \quad (2)$$

Here, lattice symmetry has been taken into account by forming symmetry-adapted expansion coefficients for equivalent clusters. Like in the general case, α in Eq. 2 enumerates all lattice-symmetry inequivalent subsets (clusters) of a full set of lattice sites, m_{α} is the number of clusters that are equivalent to α by the lattice symmetry (divided by the total number of lattice sites N), and coefficients J_{α} are the effective cluster interactions (ECI). Angle brackets designate the arithmetic average over all sets of points $i = \{q, q', \dots, q''\}$ that are equivalent to the subset represented by α through the lattice symmetry.

The averaging over the symmetry-equivalent clusters is possible due the independence of the effective cluster interactions J_α on the spin configurations in case of a two-component system. This averaging reduces the number of independent ECI coefficients. The discrete site occupation variables σ_i are usually assigned the values of +1 and -1 in a binary system.

The cluster expansions Eqs.1 and 2 converge rapidly with cluster size, and yield an exact result in the untruncated form. In this work, the CE fitting of the mixing energy and search for the thermodynamic ground state were carried out with the Alloy-Theoretic Automated Toolkit (ATAT) code.⁴⁷ The quality of the CE fit was evaluated using a cross-validation score.⁴⁸ To evaluate the relative stability, the mixing energy of $C_{1-x}N_x$ alloy (E) was defined as:

$$E = \frac{E_{\text{total}}}{n} - x\mu_N - (1-x)\mu_C$$

where the E_{total} and n are the total energy and total number of atoms of the system, μ_N and μ_C represented chemical potentials of nitrogen and carbon atoms, which were set equal to the cohesive energies of graphite and N_2 molecular crystals.⁴⁹ The mixing energies of alloy structures generated by ATAT and used in the fitting procedure were computed at the density-functional theory (DFT) level. Total energies and band structures were obtained within the local spin density approximation (LSDA) with projector-augmented wave (PAW) potentials, as implemented in VASP.⁵⁰ The plane-wave cutoff was 520 eV in all calculations. The convergence threshold was set to 10^{-4} eV in energy and 10^{-3} eV/Å in force, and cell dimensions along the z direction were 12 Å to avoid interaction between layers. The Monkhorst-Pack k-point grids are employed for Brillouin zone integration for all the structures, using approximately same k-point density for reciprocal cells of different sizes. Line mode with 21 k-points between two high-symmetry k-points is used to further investigate the electronic behavior on the basis of the equilibrium structures. The CE fitting was based on the DFT energies of 115 CN alloy structures, containing between 4 and 12 atoms. The root-mean-square deviation of the CE-fitted mixing energies from the actual values (the cross-validation score) was 18 meV for these structures, indicating a good fit. Phonon dispersions were obtained from the DFT, and high-temperature ab initio molecular dynamics (MD) calculations were performed to test structural stabilities. Force constants for phonon calculations were found by using the density functional perturbation theory (DFPT),⁵¹ as implemented in VASP. Based on the calculated force constants, phonon dispersion curves were obtained with the PHONOPY package.⁵² The original unit cells were used in constant-temperature 5ps-long DFT MD simulation runs with the time step of 1fs. In order to capture off-gamma point vibrations, additional supercell calculations were performed using density functional based tight binding molecular dynamics (DFTB-MD) with the same time step, as implemented in the DFTB+ code.⁵³

We use the cluster expansion technique in conjunction with DFT to obtain mixing energies of two-dimensional $C_{1-x}N_x$ alloys in the range of N concentrations $0 < x \leq 3/4$. The calculated and fitted mixing energies, along with the lowest-energy configurations, are shown in Fig. 2. In the stability diagram, there are three distinct regions of concentrations, viz. (1) $0 \leq x \leq 1/4$, (2) $1/4 \leq x \leq 1/2$, and (3) $1/2 \leq x$, within which the slopes of the ground state line are constant. In the first region, $0 \leq x \leq 1/4$, the ground state line is almost flat, and the mixing energy goes up to only 76 meV/atom from 16 meV/atom when N concentration increases from 0 to 1/4. In the second region $1/4 \leq x \leq 1/2$, the mixing energy goes up much faster, reaching 184 meV/atom at $x=1/3$, and 463 meV/atom at $x=1/2$. In the third region, $1/2 \leq x$, the mixing energy goes up faster still, and reaches the value of 1405 meV/atom at $x=3/4$ N concentration. The second nearest or nearest neighbor nitrogen atoms will be present in all configurations when N concentration is higher than $x=1/4$, and similarly, the nearest neighbor N-N connections cannot be avoided when $x > 1/2$. It is clear that the first increase of the slope of the ground state energy at $x=1/4$ is a consequence of the appearance of the next nearest neighbor N atoms in the alloy, and the second increase at $x=1/2$ is due to the formation of N-N bonds. Long-range interactions of N atoms in a hexagonal lattice produce a substantial, destabilizing effect on the system, and one can expect that the structural instability will appear somewhere before the formation of direct N-N bonds, i.e. at concentrations lower than 1/2.

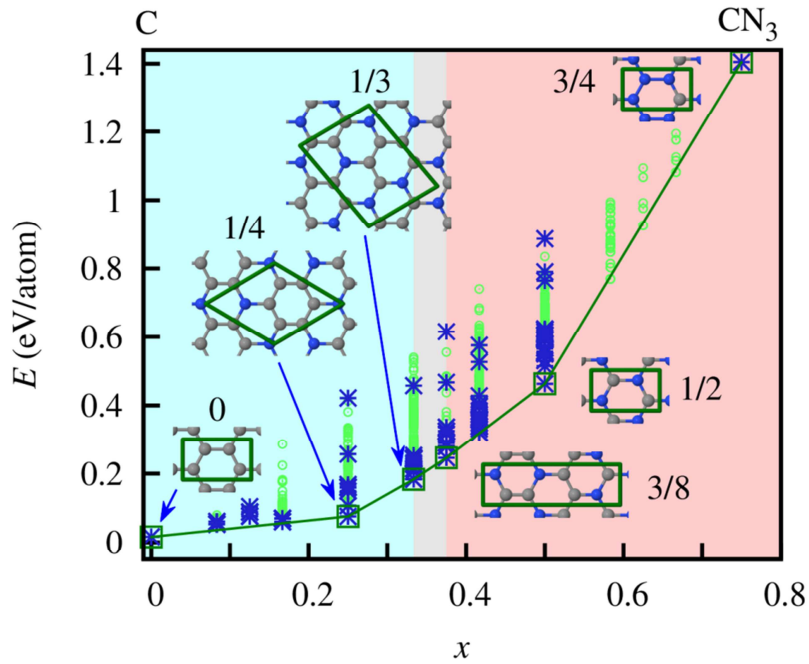


Figure 2. Mixing energies of the carbon-nitrogen two-dimensional alloy obtained with the cluster expansion. Blue stars show the DFT results, and green circles give energies obtained from the cluster expansion fitting. Squares show the values of the lowest mixing energy (ground state) at each concentration. The solid line outlines the convex hull of the mixing energies. Chemical potentials of

carbon and nitrogen atoms were set equal to the cohesive energies of graphite and N₂ molecular crystals, respectively. Units cells for the lowest energy states at N concentrations of 0, 1/4, 1/3, 3/8, 1/2 and 3/4 are shown. Predicted regions of metastability ($x < 1/3$), stability switchover ($1/3 < x < 3/8$), and instability ($x > 3/8$) are highlighted.

On the other hand, the line of the convex hull has a very slight upward slope for x between 0 and 1/4, and thus one can expect facile mixing of pure phases and good alloy stability in that range. The instability should occur in the second region, $1/4 \leq x \leq 1/2$, where second-neighbor N atoms appear. Below we describe the phonon and molecular dynamics calculations that were performed in order to test the structural stability of the lowest energy states for $0 \leq x \leq 1/4$ and also at higher concentrations. From these calculations, we predict an actual threshold N concentration at which the alloy should become unstable. Our estimate shows that the structural instability should occur around $x = 3/8$ (37.5%). Above this concentration, all graphene-like CN alloys are predicted to be unstable.

The calculated phonon spectra of the ground state structures at various concentrations are shown in Fig. 3. The structures (shown in Fig 3a-e) with low N concentrations ($x \leq 1/3$) performed good dynamics stability. Imaginary frequencies first appear at the N concentration of $x = 3/8$. All other tested structures with higher N concentrations ($x = 5/12, 1/2, 3/4$) contained imaginary phonon frequencies as well. We interpret these imaginary frequencies as indicators of the structural instability of the alloy. The concentration $x = 3/8$ (37.5%) with the mixing energy of 246 meV/atom is taken as a threshold value for instability.

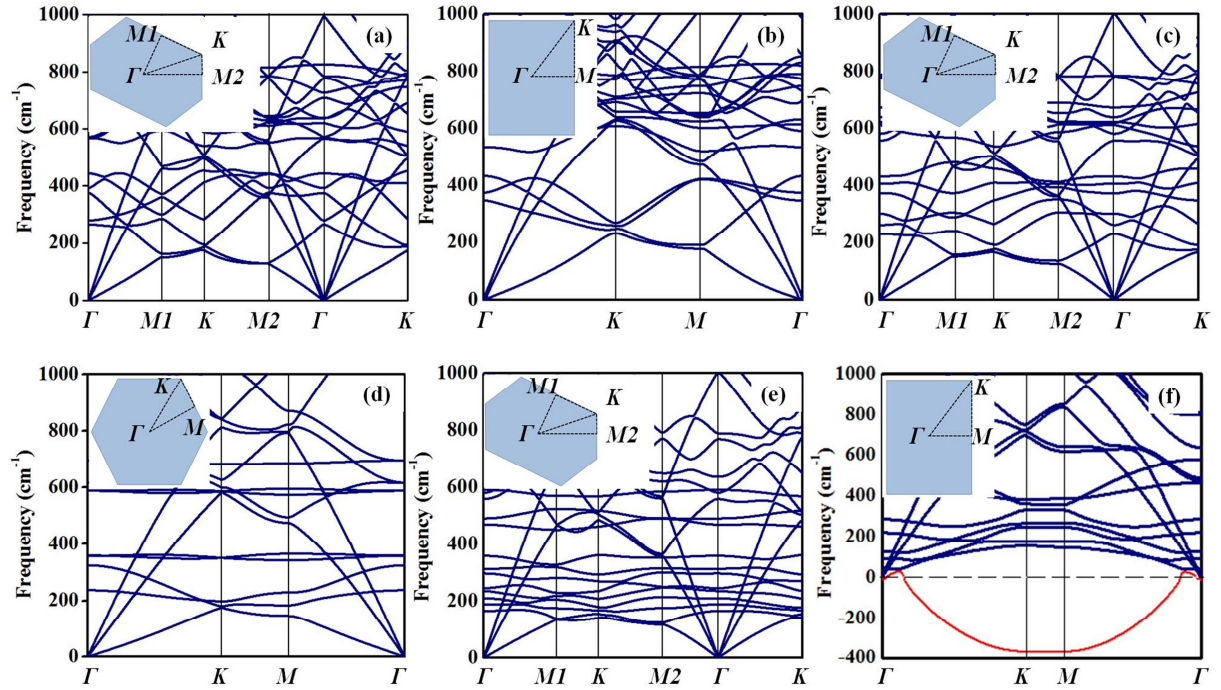


Figure 3. Calculated phonon spectra of the lowest-energy states of CN alloys at different N concentrations (a) $x=1/12$; (b) $x=1/8$; (c) $x=1/6$; (d) $x=1/4$; (e) $x=1/3$; (f) $x=3/8$. Imaginary frequencies appear at the N concentration of $x=3/8$ (37.5%) as well as all higher concentrations and marked with a red line in (f).

We next confirm the predictions of phonon calculations by testing the stability of the lowest-energy configurations with a different approach, namely high-temperature ab initio molecular dynamics based on DFT, as well as density functional tight binding (DFTB). A structure is deemed thermally stable if all atoms remain near their initial equilibrium positions at the end of the MD run. The original unit cells are used in DFT and 8×8 supercells are employed in DFTB. First, we test the structures at a relatively high temperature of 1500 K in DFT MD simulations with 5ps duration. The structures with concentrations $x=1/12$, $1/8$, $1/6$, $1/4$, $1/3$, and $3/8$ all remain stable, showing no signs of structural disruption and preserving a nearly planar geometry at the end of each MD run. When testing the lowest-energy structure with nitrogen concentration of $x=5/12$ (41.7%), the two-dimensional configuration collapse after 0.7 ps, indicating that the melting temperature of this structure is lower than 1500 K. All other structures with higher concentrations ($x=1/2$, $3/4$) also collapse in MD calculations, confirming the destabilizing effect of increased N doping, consistent with the mixing energy trends shown in Fig. 2.

At the concentration of $x=3/8$, the lowest-energy structure don't collapse in MD calculations, although its phonon spectrum contained imaginary frequencies. This is due to the fact that the off-gamma point vibrations cannot be captured by single-cell MD calculations. To address this problem, we perform

additional calculations with a larger 8×8 supercell for all of the low-energy structures using the DFTB+ code. The faster DFTB method is used because long DFT MD runs are not feasible with the supercell structures containing several hundred of atoms. The trajectories are propagated for 10 ps in DFTB runs. Our MD tests with larger cells show a general trend of decreasing thermal stability with increasing N concentration. At 1500 K, the 8×8 structures with concentrations $x=1/12$, $1/8$ and $1/6$ all remain stable. These structures will most likely be also very stable under experimental conditions, and may be the easiest to realize. In recent experiments on nitrogen graphene doping,³³ a mixing N concentration of 16.4% has been reported. The final state of the structure with concentration $x=1/6$ (16.7%) is shown in Fig. 4a. The structures with N concentrations that are higher than $1/6$ are unstable at 1500 K, as evident from Fig. 4b, which shows the final state of the structure with the concentration $x=1/4$. Xiang *et al.* have previously confirmed the stability of the $x=1/4$ structure with MD simulation at 500 K, and we have also tested this structure at temperatures of 1000 K and 500 K. Our DFTB MD results agree well with these previous calculations. Fig. 4c shows the final geometry of the $x=1/4$ configuration at 500 K, which remains planar with all the atoms near their initial equilibrium positions. However, the $x=1/3$ structure is unstable at 1500, 1000, and also 500 K. We then test this structure by performing DFTB MD simulations at 300, 200 and 100 K. The structure remain intact only at 100 K, indicating that it has a low melting point between 100 and 200 K. Fig. 4d, 4e, and 4f, show this structure at the end of the MD runs at 1500, 500, and 100 K, respectively, evidencing a more significant damage at higher temperatures. We have additionally tested the $x=3/8$ structure with supercell calculations at 100 K. After 10ps simulation, out-of-plane C pairs have been formed, in agreement with the predicted instability based on phonon calculations.

The MD calculations reveal that the mechanism that is responsible for the thermal decomposition of the CN alloy structures is the breaking of the carbon-carbon bond. This mechanism is in contrast with the expectation of the structure being weakened by its carbon-nitrogen bonds. As is well known, the sp^2 carbon-nitrogen bond is both shorter and stronger than the sp^2 carbon-carbon bond in graphene. As a result of alloying, the carbon-carbon bonds of graphene is compressed from 1.417 to 1.377 Å, as the N concentrations increases from $1/12$ to $3/8$, as shown in Table I. The strain has a greater destabilizing effect on the C-C bonds and is released by out-of-plane relaxations of carbon atoms, as seen in Fig. 4b, 4d, and 4e. Both phonon and MD calculations predict that the stability switchover in a hexagonal 2D CN alloy should occur at N concentration between $x=1/3$ (33.3%) and $x=3/8$ (37.5%).

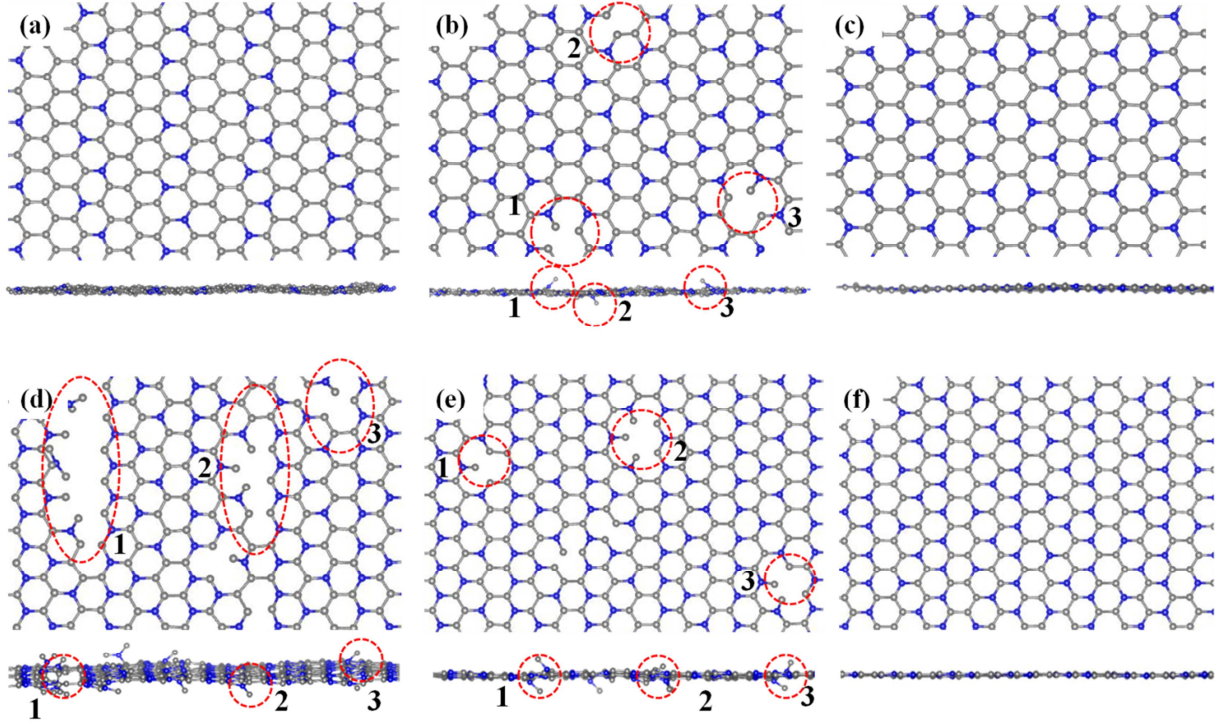


Figure 4. Top and side view of snapshots of the selected low energy 2D CN alloy structures as predicted by the cluster expansion after 10ps of the MD simulation in the NVT ensemble using a 8×8 supercell for (a) $x=1/6$ at 1500 K, (b) $x=1/4$ at 1500 K, (c) $x=1/4$ at 500 K, (d) $x=1/3$ at 1500 K, (e) $x=1/3$ at 500 K, and (f) $x=1/3$ at 100 K. The red circles mark the disrupted areas in each unstable configuration; the numbers are used to set the correspondence between the areas in the top and side views.

Table I. Calculated properties of two-dimensional CN alloys at various N concentrations: mixing energy (E), band gap, structural stability, and average length of the C-C bond.

N concentration	E (meV/atom)	Band gap (eV)	MD stability	Phonon stability	Average C-C (\AA)
1/12	53	Metal	stable	stable	1.417
1/8	77	Metal	stable	stable	1.415
1/6	61	Metal	stable	stable	1.409
1/4	76	0.37	stable	stable	1.401
1/3	184	Metal	stable	stable	1.393
3/8	246	Metal	unstable	unstable	1.377

We finally briefly address the electronic properties of the 2D CN alloys. Overall, among all considered CN structures, metallic materials dominate, with approximately 70% of structures being gapless, and 30%

semiconducting. The metallic alloys are strongly degenerate, with Fermi level located deep in the conduction band. The band structures of the most stable alloys at N concentrations of $x=1/12$, $1/8$, $1/6$, $1/4$, $1/3$, and $3/8$ are shown in Fig.5. The familiar Dirac cone feature of graphene is completely removed by alloying and thus can no longer be seen. Site-projected DOS analysis shows that the Bloch states near the Fermi level mainly originate from the C p_z orbital, with smaller contributions from the dopant N p_z states. Increasing N atom concentration from $x=1/12$ to $1/8$ to $1/6$ raises the Fermi level further into the conduction band as seen in Fig 5a, b and c. However, at N concentration of $1/4$ (Fig 5d), a special stable semiconducting structure with an indirect band gap of 0.37 eV is observed. Previous work have proposed the mechanism of band gap opening for this structure by employing Clar's rule.¹¹ In this structure, N atoms divide the graphene plane into isolated hexagonal carbon rings, which belongs to the class 1CF of the (pseudo)-all-benzenoid structures and form Clar sextets. Previously, Wassmann *et al.*⁵⁴ used the rule to explain the band gap opening in a related graphene nanoribbon structures. At even higher N concentrations of $x=1/3$ and $3/8$ as shown in Fig 5e and f, the Fermi level keeps rising into the conduction band.

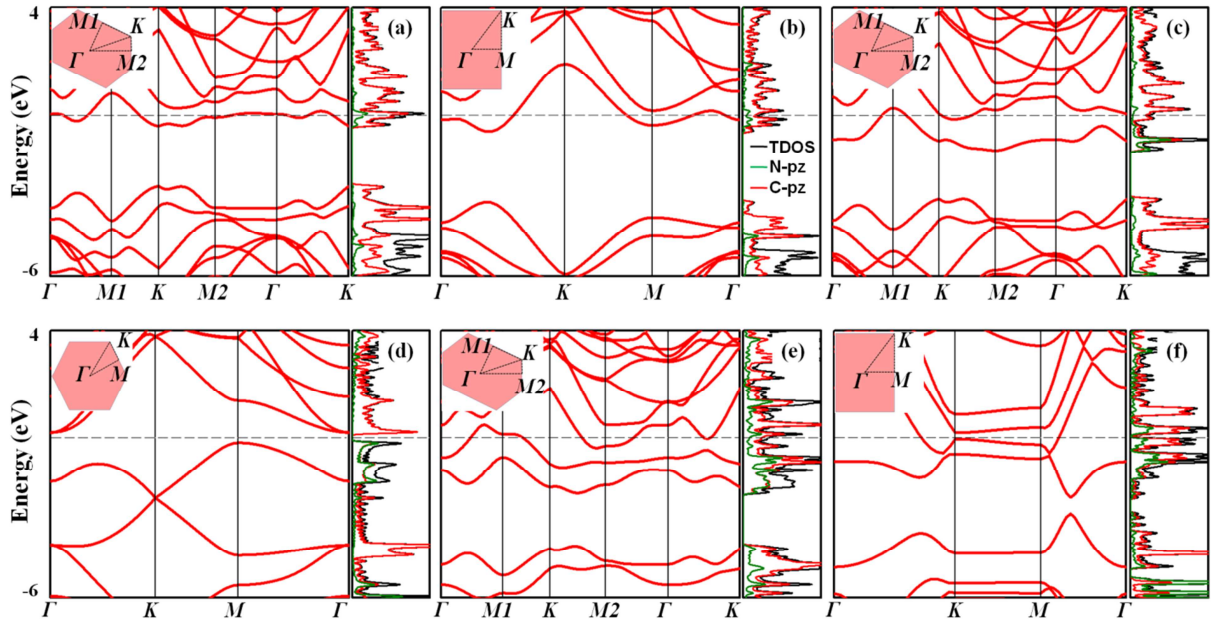


Figure 5. Electronic band structures and total and projected densities of states of stable CN alloys at different N concentrations: (a) $x=1/12$; (b) $x=1/8$; (c) $x=1/6$; (d) $x=1/4$; (e) $x=1/3$; (f) $x=3/8$.

In summary, we have studied the nitrogen doping limitations of g-NG treated as a $C_{1-x}N_x$ alloy by employing first-principle calculations and cluster expansion. We found that the largest achievable N doping concentration in g-NG is 33.3%-37.5%. Higher concentrations are not possible because of the strong repulsive interactions between nitrogen dopants. Our phonon calculations reveal that there are no imaginary frequencies in the phonon spectra for the $x \leq 1/3$ structures. These stability results have also

been confirmed by ab initio MD calculations. Low dopant concentration structures ($x \leq 1/4$) are stable at a temperature of 500 K and higher; however, the melting point of the $x=1/3$ C₂N structure is quite low, being between 100 and 200K. Most of the stable structures exhibited n-type doped metallic behavior with the exception of the special-configuration $x=1/4$ structure, which is a semiconductor. By increasing the N concentration, the Fermi level of the system is lifted into the conduction band. Our study is useful for broadening the applications of N-doped graphene in electronics and catalysis.

Acknowledgements

The authors thank Evgeni Penev for stimulating discussions. This work was supported by the U.S. Army Research Office MURI grant W911NF-11-1-0362, and in part by the Robert Welch Foundation (C-1590). Computer resources were provided by XSEDE, which is supported by NSF grant OCI-1053575, under allocation TG-DMR100029; and the DAVinCI cluster acquired with funds from NSF grant OCI-0959097.

References

- (1)Kutana, A.; Penev, E. S.; Yakobson, B. I., Engineering electronic properties of layered transition-metal dichalcogenide compounds through alloying, *Nanoscale* **2014**, *6*, 5820-5825.
- (2)Chen, Y. F.; Xi, J. Y.; Dumcenco, D. O.; Liu, Z.; Suenaga, K.; Wang, D.; Shuai, Z. G.; Huang, Y. S.; Xie, L. M., Tunable Band Gap Photoluminescence from Atomically Thin Transition-Metal Dichalcogenide Alloys, *Acs Nano* **2013**, *7*, 4610-4616.
- (3)Penev, E. S.; Bhowmick, S.; Sadrzadeh, A.; Yakobson, B. I., Polymorphism of Two-Dimensional Boron, *Nano. Lett.* **2012**, *12*, 2441-2445.
- (4)Panchokarla, L. S.; Subrahmanyam, K. S.; Saha, S. K.; Govindaraj, A.; Krishnamurthy, H. R.; Waghmare, U. V.; Rao, C. N. R., Synthesis, Structure, and Properties of Boron- and Nitrogen-Doped Graphene, *Adv. Mater.* **2009**, *21*, 4726-4731.
- (5)Wang, X. R.; Li, X. L.; Zhang, L.; Yoon, Y.; Weber, P. K.; Wang, H. L.; Guo, J.; Dai, H. J., N-Doping of Graphene Through Electrothermal Reactions with Ammonia, *Science*. **2009**, *324*, 768-771.
- (6)Zou, Y.; Li, F.; Zhu, Z. H.; Zhao, M. W.; Xu, X. G.; Su, X. Y., An ab initio study on gas sensing properties of graphene and Si-doped graphene, *Eur. Phys. J. B.* **2011**, *81*, 475-479.
- (7)Meyer, J. C.; Kurasch, S.; Park, H. J.; Skakalova, V.; Kunzel, D.; Gross, A.; Chuvilin, A.; Algara-Siller, G.; Roth, S.; Iwasaki, T. *et al.*, Experimental analysis of charge redistribution due to chemical bonding by high-resolution transmission electron microscopy, *Nat. Mater.* **2011**, *10*, 209-215.
- (8)Zhao, L. Y.; He, R.; Rim, K. T.; Schiros, T.; Kim, K. S.; Zhou, H.; Gutierrez, C.; Chockalingam, S. P.; Arguello, C. J.; Palova, L. *et al.*, Visualizing Individual Nitrogen Dopants in Monolayer Graphene, *Science*. **2011**, *333*, 999-1003.
- (9)Dai, J. Y.; Yuan, J. M.; Giannozzi, P., Gas adsorption on graphene doped with B, N, Al, and S: A theoretical study, *Appl. Phys. Lett.* **2009**, *95*, 232105.
- (10)Lv, R.; Li, Q.; Botello-Mendez, A. R.; Hayashi, T.; Wang, B.; Berkdemir, A.; Hao, Q. Z.; Elias, A. L.; Cruz-Silva, R.; Gutierrez, H. R. *et al.*, Nitrogen-doped graphene: beyond single substitution and enhanced molecular sensing, *Sci. Rep.* **2012**, *2*, 586-593.
- (11)Xiang, H. J.; Huang, B.; Li, Z. Y.; Wei, S. H.; Yang, J. L.; Gong, X. G., Ordered Semiconducting Nitrogen-Graphene Alloys, *Phys. Rev. X* **2012**, *2*, 011003
- (12)Liu, A. Y.; Wentzcovitch, R. M.; Cohen, M. L., Atomic Arrangement and Electronic-Structure of Bc₂n, *Phys. Rev. B.* **1989**, *39*, 1760-1765.
- (13)Raidongia, K.; Nag, A.; Hembram, K. P. S. S.; Waghmare, U. V.; Datta, R.; Rao, C. N. R., BCN: A Graphene Analogue with Remarkable Adsorptive Properties, *Chem-Eur. J.* **2010**, *16*, 149-157.
- (14)Lam, K. T.; Lu, Y. H.; Feng, Y. P.; Liang, G. C., Stability and electronic structure of two dimensional C-x(BN)(y) compound, *Appl. Phys. Lett.* **2011**, *98*, 022101.
- (15)Zhu, J.; Bhandary, S.; Sanyal, B.; Ottosson, H., Interpolation of Atomically Thin Hexagonal Boron Nitride and Graphene: Electronic Structure and Thermodynamic Stability in Terms of All-Carbon Conjugated Paths and Aromatic Hexagons, *J. Phys. Chem. C.* **2011**, *115*, 10264-10271.
- (16)Luo, X. Y.; Yang, J. H.; Liu, H. Y.; Wu, X. J.; Wang, Y. C.; Ma, Y. M.; Wei, S. H.; Gong, X. G.; Xiang, H. J., Predicting Two-Dimensional Boron-Carbon Compounds by the Global Optimization Method, *J. Am. Chem. Soc.* **2011**, *133*, 16285-16290.
- (17)Wu, X. J.; Dai, J.; Zhao, Y.; Zhuo, Z. W.; Yang, J. L.; Zeng, X. C., Two-Dimensional Boron Monolayer Sheets, *Acs Nano* **2012**, *6*, 7443-7453.
- (18)Kumar, N.; Moses, K.; Pramoda, K.; Shirodkar, S. N.; Mishra, A. K.; Waghmare, U. V.; Sundaresan, A.; Rao, C. N. R., Borocarbonitrides, B_xC_yN_z, *J. Mater. Chem. A.* **2013**, *1*, 5806-5821.
- (19)Kota Moses, S. N. S., U V Waghmare and C N R Rao, Composition-dependent photoluminescence and electronic structure of 2-dimensional borocarbonitrides, B_xC_yN_z (x = 1, 5), *Materials Research Express* **2014**, *1*, 025603.
- (20)Song, L.; Ci, L. J.; Lu, H.; Sorokin, P. B.; Jin, C. H.; Ni, J.; Kvashnin, A. G.; Kvashnin, D. G.; Lou, J.; Yakobson, B. I. *et al.*, Large Scale Growth and Characterization of Atomic Hexagonal Boron Nitride Layers, *Nano. Lett.* **2010**, *10*, 3209-3215.

- (21)Ci, L.; Song, L.; Jin, C. H.; Jariwala, D.; Wu, D. X.; Li, Y. J.; Srivastava, A.; Wang, Z. F.; Storr, K.; Balicas, L. *et al.*, Atomic layers of hybridized boron nitride and graphene domains, *Nat. Mater.* **2010**, *9*, 430-435.
- (22)Menezes, M. G.; Capaz, R. B., Half-metallicity induced by charge injection in hexagonal boron nitride clusters embedded in graphene, *Phys. Rev. B.* **2012**, *86*, 195413.
- (23)Kawaguchi, M.; Kawashima, T.; Nakajima, T., Syntheses and structures of new graphite-like materials of composition BCN(H) and BC₃N(H), *Chem. Mater.* **1996**, *8*, 1197-1201.
- (24)Cui, T. X.; Lv, R. T.; Huang, Z. H.; Zhu, H. W.; Zhang, J.; Li, Z.; Jia, Y.; Kang, F. Y.; Wang, K. L.; Wu, D. H., Synthesis of nitrogen-doped carbon thin films and their applications in solar cells, *Carbon.* **2011**, *49*, 5022-5028.
- (25)Lv, R. T.; Cui, T. X.; Jun, M. S.; Zhang, Q.; Cao, A. Y.; Su, D. S.; Zhang, Z. J.; Yoon, S. H.; Miyawaki, J.; Mochida, I. *et al.*, Open-Ended, N-Doped Carbon Nanotube-Graphene Hybrid Nanostructures as High-Performance Catalyst Support, *Adv. Funct. Mater.* **2011**, *21*, 999-1006.
- (26)Qu, L. T.; Liu, Y.; Baek, J. B.; Dai, L. M., Nitrogen-Doped Graphene as Efficient Metal-Free Electrocatalyst for Oxygen Reduction in Fuel Cells, *Acs Nano* **2010**, *4*, 1321-1326.
- (27)Tang, Z. W.; Chen, X. W.; Chen, H.; Wu, L. M.; Yu, X. B., Metal-Free Catalysis of Ammonia-Borane Dehydrogenation/Regeneration for a Highly Efficient and Facilely Recyclable Hydrogen-Storage Material, *Angew. Chem. Int. Edit.* **2013**, *52*, 5832-5835.
- (28)Reddy, A. L. M.; Srivastava, A.; Gowda, S. R.; Gullapalli, H.; Dubey, M.; Ajayan, P. M., Synthesis Of Nitrogen-Doped Graphene Films For Lithium Battery Application, *Acs Nano* **2010**, *4*, 6337-6342.
- (29)Lu, R. F.; Meng, Z. S.; Rao, D. W.; Wang, Y. H.; Shi, Q.; Zhang, Y. D.; Kan, E. J.; Xiao, C. Y.; Deng, K. M., A promising monolayer membrane for oxygen separation from harmful gases: nitrogen-substituted polyphenylene, *Nanoscale* **2014**, *6*, 9960-9964.
- (30)Jeong, H. M.; Lee, J. W.; Shin, W. H.; Choi, Y. J.; Shin, H. J.; Kang, J. K.; Choi, J. W., Nitrogen-Doped Graphene for High-Performance Ultracapacitors and the Importance of Nitrogen-Doped Sites at Basal Planes, *Nano. Lett.* **2011**, *11*, 2472-2477.
- (31)Jin, Z.; Yao, J.; Kittrell, C.; Tour, J. M., Large-Scale Growth and Characterizations of Nitrogen-Doped Monolayer Graphene Sheets, *Acs Nano* **2011**, *5*, 4112-4117.
- (32)Wei, D. C.; Liu, Y. Q.; Wang, Y.; Zhang, H. L.; Huang, L. P.; Yu, G., Synthesis of N-Doped Graphene by Chemical Vapor Deposition and Its Electrical Properties, *Nano. Lett.* **2009**, *9*, 1752-1758.
- (33)Deng, D. H.; Pan, X. L.; Yu, L. A.; Cui, Y.; Jiang, Y. P.; Qi, J.; Li, W. X.; Fu, Q. A.; Ma, X. C.; Xue, Q. K. *et al.*, Toward N-Doped Graphene via Solvothermal Synthesis, *Chem. Mater.* **2011**, *23*, 1188-1193.
- (34)Zabet-Khosousi, A.; Zhao, L. Y.; Palova, L.; Hybertsen, M. S.; Reichman, D. R.; Pasupathy, A. N.; Flynn, G. W., Segregation of Sublattice Domains in Nitrogen-Doped Graphene, *J. Am. Chem. Soc.* **2014**, *136*, 1391-1397.
- (35)Usachov, D.; Vilkov, O.; Gruneis, A.; Haberer, D.; Fedorov, A.; Adamchuk, V. K.; Preobrajenski, A. B.; Dudin, P.; Barinov, A.; Oehzelt, M. *et al.*, Nitrogen-Doped Graphene: Efficient Growth, Structure, and Electronic Properties, *Nano. Lett.* **2011**, *11*, 5401-5407.
- (36)Gopalakrishnan, K.; Govindaraj, A.; Rao, C. N. R., Extraordinary supercapacitor performance of heavily nitrogenated graphene oxide obtained by microwave synthesis, *J. Mater. Chem. A.* **2013**, *1*, 7563-7565.
- (37)Sandoval, S.; Kumar, N.; Sundaresan, A.; Rao, C. N. R.; Fuertes, A.; Tobias, G., Enhanced Thermal Oxidation Stability of Reduced Graphene Oxide by Nitrogen Doping, *Chem-Eur. J.* **2014**, *20*, 11999-12003.
- (38)Wang, X.; Maeda, K.; Thomas, A.; Takanabe, K.; Xin, G.; Carlsson, J. M.; Domen, K.; Antonietti, M., A metal-free polymeric photocatalyst for hydrogen production from water under visible light, *Nat Mater* **2009**, *8*, 76-80.
- (39)Wood, K. N.; O'Hayre, R.; Pylypenko, S., Recent progress on nitrogen/carbon structures designed for use in energy and sustainability applications, *Energy Environ. Sci.* **2014**, *7*, 1212-1249.
- (40)Lee, J. S.; Wang, X.; Luo, H.; Dai, S., Fluidic Carbon Precursors for Formation of Functional Carbon under Ambient Pressure Based on Ionic Liquids, *Advanced Materials* **2010**, *22*, 1004-1007.

- (41) Lu, R.; Meng, Z.; Rao, D.; Wang, Y.; Shi, Q.; Zhang, Y.; Kan, E.; Xiao, C.; Deng, K., A promising monolayer membrane for oxygen separation from harmful gases: nitrogen-substituted polyphenylene, *Nanoscale* **2014**, *6*, 9960-9964.
- (42) Lu, R.; Meng, Z.; Kan, E.; Li, F.; Rao, D.; Lu, Z.; Qian, J.; Xiao, C.; Wu, H.; Deng, K., Tunable band gap and hydrogen adsorption property of a two-dimensional porous polymer by nitrogen substitution, *Phys. Chem. Chem. Phys.* **2013**, *15*, 666-670.
- (43) Liu, H. T.; Liu, Y. Q.; Zhu, D. B., Chemical doping of graphene, *J. Mater. Chem.* **2011**, *21*, 3335-3345.
- (44) Lherbier, A.; Blase, X.; Niquet, Y. M.; Triozon, F.; Roche, S., Charge transport in chemically doped 2D graphene, *Phys. Rev. Lett.* **2008**, *101*, 306808.
- (45) Schiros, T.; Nordlund, D.; Palova, L.; Prezzi, D.; Zhao, L. Y.; Kim, K. S.; Wurstbauer, U.; Gutierrez, C.; Delongchamp, D.; Jaye, C. *et al.*, Connecting Dopant Bond Type with Electronic Structure in N-Doped Graphene, *Nano. Lett.* **2012**, *12*, 4025-4031.
- (46) Sanchez, J. M.; Ducastelle, F.; Gratias, D., Generalized Cluster Description of Multicomponent Systems, *Physica A* **1984**, *128*, 334-350.
- (47) van de Walle, A.; Asta, M.; Ceder, G., The Alloy Theoretic Automated Toolkit: A user guide, *Calphad Alloy Thermodyn., Proc. Symp.* **2002**, *26*, 539-553.
- (48) van de Walle, A.; Ceder, G., Automating first-principles phase diagram calculations, *J. Phase Equilib.* **2002**, *23*, 348-359.
- (49) Scott, T. A., Solid and liquid nitrogen, *Phys. Rep.* **1976**, *3*, 89-157.
- (50) Kresse, G.; Furthmuller, J., Efficient iterative schemes for ab initio total-energy calculations using a plane-wave basis set, *Phys. Rev. B.* **1996**, *54*, 11169-11186.
- (51) Baroni, S.; de Gironcoli, S.; Dal Corso, A.; Giannozzi, P., Phonons and related crystal properties from density-functional perturbation theory, *Rev. Mod. Phys.* **2001**, *73*, 515-562.
- (52) Togo, A.; Oba, F.; Tanaka, I., First-principles calculations of the ferroelastic transition between rutile-type and CaCl₂-type SiO₂ at high pressures, *Phys. Rev. B.* **2008**, *78*, 134106.
- (53) Aradi, B.; Hourahine, B.; Frauenheim, T., DFTB+, a sparse matrix-based implementation of the DFTB method, *J. Phys. Chem. A.* **2007**, *111*, 5678-5684.
- (54) Wassmann, T.; Seitsonen, A. P.; Saitta, A. M.; Lazzeri, M.; Mauri, F., Clar's Theory, π -Electron Distribution, and Geometry of Graphene Nanoribbons, *J. Am. Chem. Soc.* **2010**, *132*, 3440-3451.